ARTICLE

Selective electrochemical capture and release of uranyl from aqueous alkali, lanthanide, and actinide mixtures using redox-switchable carboranes

Megan Keener,[a‡] Maxwell Mattejat,[a‡] Shao-Liang Zheng,[b] Guang Wu,[a] Trevor W. Hayton[a] and Gabriel Ménard*[a]

We report the selective electrochemical biphasic capture of the uranyl cation (UO_2^{2+}) from mixed-metal alkali (Cs^+), lanthanide (Nd^{3+}, Sm^{3+}), and actinide (Th^{4+}, UO_2^{2+}) aqueous solutions to an organic, 1,2-dichloroethane (DCE), phase using the *ortho*-substituted *nido*-carborane anion, $[1,2-(Ph_2PO)_2-1,2-C_2B_{10}H_{10}]^{2-}$ (**$^{PO}Cb^{2-}$**). The reduced **$^{PO}Cb^{2-}$** is generated by electrochemical reduction of the *closo*-carborane, **^{PO}Cb**, prior to mixing with the aqueous mixed-metal solution. Subsequent UO_2^{2+} release from the captured product, **$[UO_2(^{PO}Cb)_2]^{2-}$**, was performed by galvanostatic bulk electrolysis of the DCE phase and back-extraction of UO_2^{2+} to a fresh aqueous phase. The selective capture and release of UO_2^{2+} was confirmed by combined ICP-OES and NMR spectral analyses of the aqueous and organic phases, respectively, against the newly synthesized *nido*-carborane complexes, **$[[CoCp^*_2][Cs(^{PO}Cb)]]_2$**, **$[CoCp^*_2]_3[Nd(^{PO}Cb)_3]$**, **$[CoCp^*_2]_3[Sm(^{PO}Cb)_3]$**, and **$[CoCp^*_2]_2[Th(^{PO}Cb)_3]$**.

Introduction

With over 440 operational reactors worldwide, nuclear energy currently provides 11% of all electricity. Several countries have proposed to increase nuclear energy production to meet their Paris Agreement targets for decarbonizing their economies, with the most ambitious being India and China that propose eight- and five-fold increases in domestic nuclear capacity, respectively.[1] While nuclear energy is often considered a low-carbon energy alternative to fossil fuels,[2, 3] the disposal of spent nuclear fuel (SNF), as well as the inadvertent release of radioactive material to the environment (*e.g.*, release of ^{137}Cs at Chernobyl and Fukushima), make this technology imperfect.

Uranium, in its dioxide form (UO_2), is both the main component in nuclear fuel, as well as SNF, where the concentration drops to approximately 95%. New fission products generated include: Pu (0.9%); the minor actinides (0.1% (Np, Am, Cm)); lanthanides, Tc, Mo, I, Cs and others (together ca. 4%).[4] As of 2020, approximately 450,000 tons of SNF have been cumulatively generated worldwide, of which only ~ 25% have been reprocessed using the decades-old Plutonium Uranium Redox EXtraction (PUREX) process.[5] While this commercial, liquid-liquid process is extremely efficient at extracting and recycling UO_2^{2+} using stoichiometric extractants,

in turn reducing SNF loads, PUREX involves the selective extraction of a pure Pu stream which raises significant proliferation concerns from major stakeholders, such as the U.S.[6] While other reprocessing schemes addressing these concerns have been developed (*e.g.*, UREX), none are commercial. To this day, proliferation concerns have superseded reprocessing efforts in places like the U.S., forcing countries to instead increase their SNF storage capacity, thus deferring action on the nuclear waste issue.[4, 6, 7] New strategies for the selective separation and recovery of UO_2^{2+} from SNF, without the parallel extraction of a Pu stream, could therefore significantly aid in reducing net SNF generated from reactors, minimizing demands on long-term geological repositories, and in turn closing the fuel cycle.

We recently reported a new, biphasic, electro/chemical method for capturing UO_2^{2+} using the *ortho*-substituted *nido*-carborane anion, $[1,2-(Ph_2PO)_2-1,2-C_2B_{10}H_{10}]^{2-}$ (**$^{PO}Cb^{2-}$**) generating the captured species, **$[UO_2X_n(^{PO}Cb)_{(2-n/2)}]^{2-}$** (n = 0, 2; X = Cl, OAc; Fig. 1a). Electrochemical oxidation of this species was initiated to generate the oxidized *closo*-carborane (**^{PO}Cb**), initiating the release of UO_2^{2+} to the aqueous layer. Repeated capture and release of UO_2^{2+} in monophasic organic solution further demonstrated the potential applicability and recyclability of this extractant.[8] In this study, we wanted to explore the *selective* biphasic capture and release of UO_2^{2+} using the **$^{PO}Cb^{2-}$**/**^{PO}Cb** system from aqueous solutions of alkali, lanthanide, and actinide metals more closely mimicking SNF streams. The choice of metals, and the reasons for using each, are as follows: 1) natural abundance $^{133}Cs^+$ (100%) was used to mimic the highly radiotoxic ^{137}Cs isotope which is responsible for much of the human health, environmental, and hot SNF disposal issues[7, 9, 10]; 2) Nd^{3+} and Sm^{3+} were chosen due to their

[a.] Department of Chemistry and Biochemistry, University of California, Santa Barbara, California 93106, United States

[b.] Department of Chemistry and Chemical Biology, Harvard University, Cambridge, Massachusetts 02138, United States

‡These authors contributed equally to this work.

abundance in SNF[7]; 3) Th^{4+} was used due to its abundance in SNF,[7] and also because it functions as a Pu^{4+} surrogate in light of our inability to handle this highly controlled element in house.[11-13] Herein, we describe both the coordination chemistry of $^{PO}Cb^{2-}$ to these individual metals, as well as the *highly selective* electrochemical capture of UO_2^{2+} with $^{PO}Cb^{2-}$ from the mixed-metal aqueous solution to an organic phase. The electrochemical release of UO_2^{2+} to a fresh aqueous phase is also described (Fig. 1b).

a) Previous work
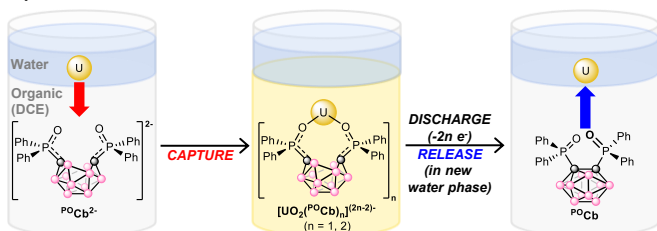
b) This work
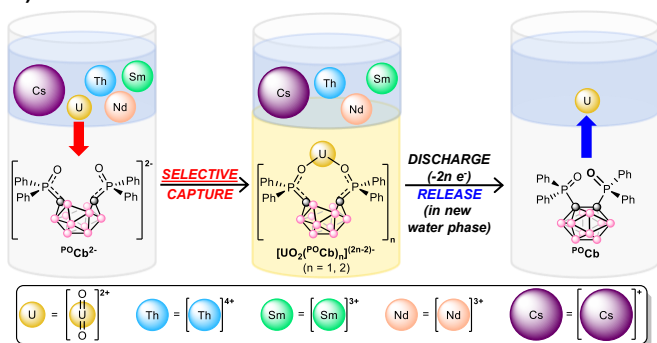
Fig. 1 a) Our previous work demonstrating the biphasic, electrochemical capture and release of UO_2^{2+} using the $^{PO}Cb^{2-}/^{PO}Cb$ system. b) This work highlighting the *selective* capture and release of UO_2^{2+} from aqueous solutions containing alkali, lanthanide, and actinide metals.

Results and discussion

The coordination chemistry of the $^{PO}Cb^{2-}$ ligand was investigated using the previously reported $[CoCp^*_2]^+$ salt, $[CoCp^*_2]_2[^{PO}Cb]$ $(Cp^* = \eta^5\text{-}C_5Me_5)$,[8] in tandem with the nitrate salts of Cs^+, Nd^{3+}, Sm^{3+}, and Th^{4+}. All complexes were synthesized following an analogous synthetic procedure in MeCN. The Cs complex was

generated by addition of an equimolar solution of $[CoCp^*_2]_2[^{PO}Cb]$ to a solution of $CsNO_3$ in MeCN at r.t. Following the selective recrystallization and separation of the $[CoCp^*_2][NO_3]$ byproduct, the desired product was isolated and unambiguously identified by single crystal X-ray diffraction (XRD) studies as the dimeric salt, $[[CoCp^*_2][Cs(^{PO}Cb)]]_2$ (Fig. 2a). The symmetric dimer features a central diamond-shaped core structure with two Cs atoms at the apical positions held in place by oxide donors from each ligand (Cs1–O(1, 1') = 2.9893(18), 3.0844(19) Å), as well as Cs–H–B bonds[14, 15] (Cs1–B(3, 3') = 3.681(3), 3.631(3) Å; Cs1–H(3, 3') = 2.924, 3.08(3) Å). Other interactions outside the diamond core are provided by the additional oxide donor (Cs1–O2 = 2.9356(18) Å), as well as an additional B contact (Cs1–B4' = 3.726(3) Å). We note that a Cs–H (3.199 Å) contact arising from a phenyl *meta*-C–H bond of an adjacent dimer is also observed, generating a polymeric structure (see Fig. S7 (not shown in Fig. 2a)). The *nido* $^{PO}Cb^{2-}$ ligand charged state is maintained as indicated by the long C1–C2 distance (2.862 Å),[8] which is well outside the range of a C–C bond. Together, we tentatively assign a coordination number (CN) of 9 to the large Cs cation. Due to the imposed crystal symmetry, identical bond metrics are found for Cs1'. The bonding types and lengths, the polymeric structure, and the assigned CN are similar to previously reported data for Cs.[14-17] Lastly, while the solid-state structure displays inequivalent P=O donor groups in the $^{PO}Cb^{2-}$ ligands, we note that the diamagnetic complex displays a single resonance in the ^{31}P NMR spectrum at 31.7 ppm in MeCN-d_3 indicating higher symmetry in solution, perhaps due to the breakup of the polymeric structure initiated by the coordinating solvent (Fig. S10).

The lanthanide (Nd^{3+}, Sm^{3+}) and actinide (Th^{4+}) complexes were next synthesized using an identical procedure. Three equivalents of $[CoCp^*_2]_2[^{PO}Cb]$ were added to one equivalent of $M(NO_3)_n$ (M = Nd, Sm (n = 3); Th (n = 4)) in MeCN at r.t. The $[CoCp^*_2][NO_3]$ byproduct was again selectively crystallized and separated prior to isolation of the final products, which were all unambiguously identified by single crystal XRD studies as: $[CoCp^*_2]_3[Nd(^{PO}Cb)_3]$ (Fig. S8); $[CoCp^*_2]_3[Sm(^{PO}Cb)_3]$ (Fig. S9), and; $[CoCp^*_2]_2[Th(^{PO}Cb)_3]$ (Fig. 2b). All complexes have a central 6-coordinate metal center in pseudo-octahedral geometries. Average M–O bond distances of 2.327 Å (Nd), 2.315 Å (Sm), and 2.297 Å (Th) are similar to reported values[18-24] and follow an expected periodic trend based on decreasing ionic radii and
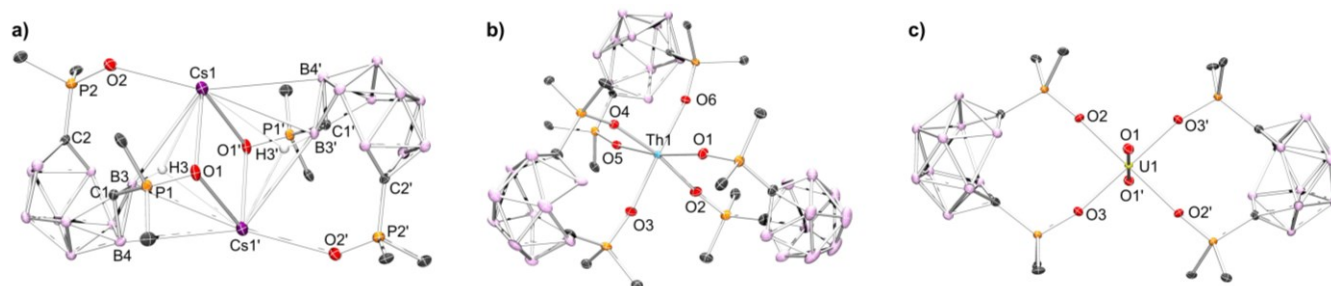

Fig. 2 Solid-state molecular structures obtained by XRD studies of: (a) $[[CoCp^*_2][Cs(^{PO}Cb)]]_2$; (b) $[CoCp^*_2]_2[Th(^{PO}Cb)_3]$, and; (c) $[CoCp^*_2]_2[UO_2(^{PO}Cb)_2]$.[8] $[CoCp^*_2]^+$ counter cations, phenyl C–H linkages, co-crystallized solvent molecules, and all H atoms, except those shown in (a), are omitted for clarity. Pertinent bond lengths and angles are discussed in the manuscript. The polymeric structure of $[[CoCp^*_2][Cs(^{PO}Cb)]]_2$ (a), filling an additional coordination site at Cs, is shown in Fig. S7.

increasing ionic charge (for Th). Long carborane C–C distances (average 2.86 Å) in each case are again indicative of a *nido* **POCb²⁻** configuration.[8] The solid-state structure of the previously reported uranyl complex, **[CoCp*₂]₂[UO₂(POCb)₂]**, is also shown in Fig. 2c as a comparison to the new complexes reported here.[8] Spectroscopically, **[CoCp*₂]₃[Nd(POCb)₃]** and **[CoCp*₂]₃[Sm(POCb)₃]** display ^{31}P NMR resonances at 140.6 and 27.9 ppm, respectively. These values are notably different from each other, likely due to their varying paramagnetism. These values are also much different from the diamagnetic **[CoCp*₂]₂[Th(POCb)₃]** (51.3 ppm) and **[CoCp*₂]₂[UO₂(POCb)₂]** (52.0 ppm) complexes.[8]

Building on our previous work (Fig. 1a),[8] we investigated the selective electrochemical capture of UO_2^{2+} from mixed aqueous alkali (Cs⁺), lanthanide (Nd³⁺, Sm³⁺), and actinide (Th⁴⁺, UO_2^{2+}) solutions mimicking in part SNF. Mixed-metal aqueous stock solutions were first prepared by dissolving equimolar quantities of the common starting materials, $CsNO_3$, $Nd(NO_3)_3(THF)_3$, $Sm(NO_3)_3(THF)_3$, $Th(NO_3)_4(H_2O)_x$, and $UO_2(NO_3)_2(THF)_2$ in Milli-Q deionized water, either with a NaOAc buffer (0.5 M, pH = 5.2) or without (pH = 2.6). The buffer in the former was used for two reasons: 1) to mimic our previous results which required the use of a buffer to control for the pH-dependent extinction coefficient (ε) of UO_2^{2+} which was monitored by UV-Vis spectroscopy,[8, 25, 26] and; 2) to compare the extraction efficacy of our system at varying pH values. In contrast to our previous work, we used inductively-coupled plasma optical emission

spectrometry (ICP-OES) to directly, and more accurately, measure trace metal concentrations in the aqueous phases pre-extraction (pre-X), post-extraction (post-X), and following back-extraction (back-X, *vide infra*).

Three separate 1,2-dichloroethane (DCE) solutions were next loaded with **POCb** (1 equiv), [PPN][PF₆] (0.5 equiv; [PPN]⁺ = [Ph₃P=N=PPh₃]⁺) as internal standard for NMR spectroscopy (*vide infra*), and [Bu₄N][PF₆] (0.1 M) as supporting electrolyte, and were loaded into one of two compartments of divided H-cells. Each counter compartment was loaded with a heterogeneous carbon additive (Ketjenblack) which served as a capacitive buffer[8, 27] and which was mixed in DCE with 0.1 M [Bu₄N][PF₆]. All H-cells were configured with physical glass-frit separators and contained reticulated vitreous carbon electrodes on each side (see SI for full experimental detail and H-cell setup). We note that each of these experiments were run in triplicate. The **POCb** solutions were electrochemically reduced by galvanostatic bulk electrolysis (GBE) to a theoretical state-of-charge (SOC) of ca. 77% assuming a 100 % coulombic efficiency (Fig. S5). Subsequent analyses of the carborane solutions by unlocked $^{31}P\{^1H\}$ NMR spectroscopy revealed the clean conversion of **POCb** to the reduced *nido*-carborane, **POCb²⁻**, each in approximate 76% yield and in line with the SOC. We note a loss of ca. 10% of combined carborane resonances (**POCb** and **POCb²⁻**) following charging and relative to the starting solutions and internal standard, perhaps due to ill-defined
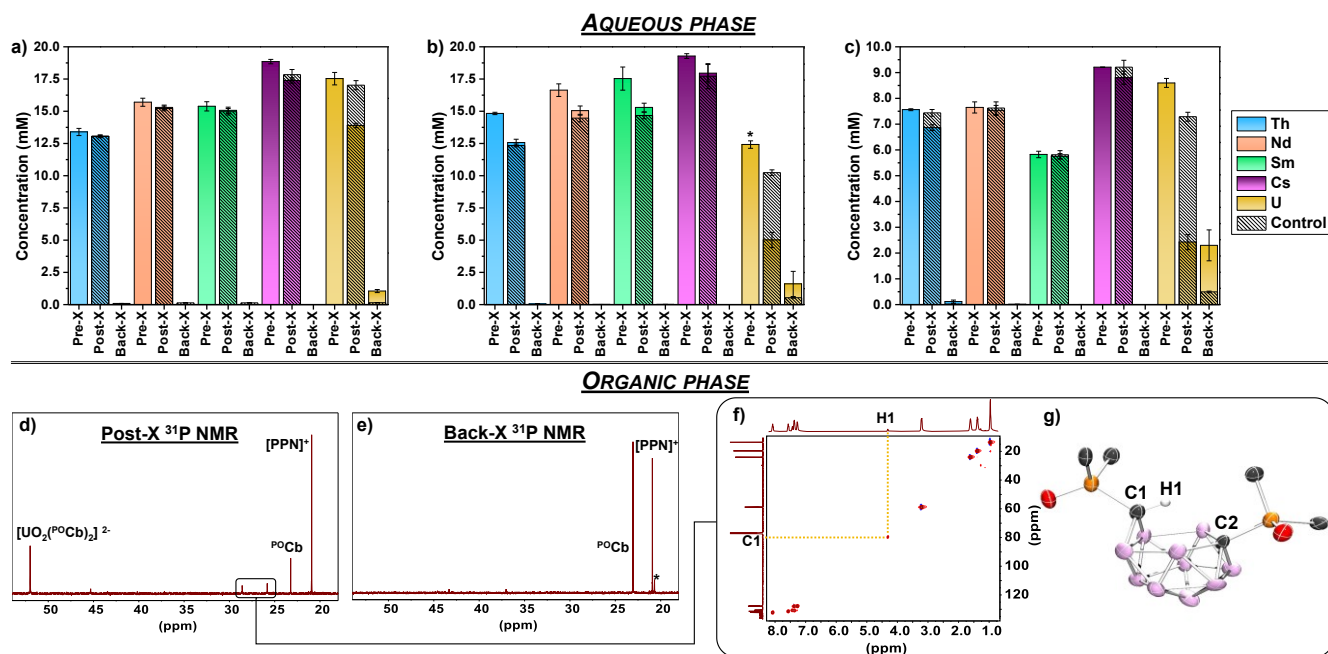
Fig. 3 ICP-OES, spectroscopic, and crystallographic data for the selective electrochemical capture and release of UO_2^{2+} from mixed-metal (Cs⁺, Nd³⁺, Sm³⁺, Th⁴⁺, UO_2^{2+}) aqueous solutions using the **POCb/POCb²⁻** system in DCE. (a-c) Average concentrations (from triplicate runs) of each metal species initially (pre-X) and following post-X and back-X using the following conditions and assuming 1.0 equiv of **POCb²⁻**: (a) a non-buffered (pH = 2.6) aqueous mixed-metal solution with ca. 1.25 equiv of each metal; (b) a NaOAc-buffered (pH = 5.2) aqueous mixed-metal solution with ca. 1.25 equiv of each metal (*slightly lower for UO_2^{2+} due to saturation concentration); (c) a NaOAc-buffered (pH = 5.2) aqueous mixed-metal solution with ca. 0.6 equiv of each metal. (d) Representative $^{31}P\{^1H\}$ NMR spectrum of the DCE layer following post-X of UO_2^{2+} from the aqueous, buffered mixed-metal solution (0.6 equiv). No resonances attributable to Cs⁺, Nd³⁺, Sm³⁺, or Th⁴⁺ extraction are present. (e) Representative $^{31}P\{^1H\}$ NMR spectrum of the DCE layer following GBE and UO_2^{2+} back-X to a fresh, buffered aqueous phase (*unknown by-product). (f) ^1H-^{13}C HSQC NMR spectrum of

[Bu₄N][^{PO}CbH] in CDCl₃ revealing C1–H1 correlation. (g) Solid-state molecular structure obtained by XRD studies of **[Bu₄N][^{PO}CbH]** ([Bu₄N]⁺ counter cation, phenyl C–H linkages, and all H atoms, except H1, are omitted for clarity).

electrochemical side reactions. Each charged solution was then removed from its respective H-cell and mixed with either: 1) a non-buffered (pH = 2.6) aqueous mixed-metal solution with ca. 1.25 equiv of each metal relative to ^{PO}Cb²⁻ (Fig. 3a); 2) a NaOAc-buffered (pH = 5.2) aqueous mixed-metal solution with ca. 1.25 equiv of each metal relative to ^{PO}Cb²⁻ (Fig. 3b), or; 3) a NaOAc-buffered (pH = 5.2) aqueous mixed-metal solution with ca. 0.60 equiv of each metal relative to ^{PO}Cb²⁻ (Fig. 3c). Significant yellowing of the organic phases was observed after 1.5 h of rapid biphasic mixing (Fig. 1b).

The aqueous mixed-metal phases were analyzed by ICP-OES prior to mixing with the organic phases (pre-X), following biphasic mixing (post-X), as well as following back-X (*vide infra*). Analysis of the non-buffered solution (Fig. 3a) post-X revealed an average decrease in UO_2^{2+} concentration of 20.7%, with minimal observed changes to the concentrations of Th^{4+}, Nd^{3+}, Sm^{3+}, and Cs^+ relative to pre-X. The minor decreases in the concentrations of these latter metals were within error to the observed changes in the controls, which were performed in parallel using identical aqueous and organic solutions (but without added ^{PO}Cb or ^{PO}Cb²⁻), as observed by the hashed bars in Fig. 3a-c. In contrast to this non-buffered solution, analysis of the buffered solution containing ca. 1.25 equiv of each metal (Fig. 3b) post-X revealed an improved extraction of UO_2^{2+} with an average decrease in concentration of 59.7% relative to pre-X (note that the pre-X [UO_2^{2+}] reached saturation here at a slightly lower concentration than the other metals). While extraction of Th^{4+}, Nd^{3+}, Sm^{3+}, and Cs^+ also increased here relative to the non-buffered solution, the observed changes were again within error and consistent with the control experiments, thus suggesting that the observed extraction of these ions was not driven by coordination to ^{PO}Cb²⁻. We next probed the effect of modifying the ^{PO}Cb²⁻:metal ratios. We note that the observed ratios of ^{PO}Cb²⁻:UO_2^{2+} are either 1:1[8] (Cs⁺ also, Fig. 2a) or 2:1 (Fig. 2c), whereas all other complexes reported here (Th^{4+}, Sm^{3+}, Nd^{3+}) are 3:1. Reducing the mixed-metal aqueous buffered solution concentration to ca. 0.6 equiv of each metal to ^{PO}Cb²⁻ revealed an increased post-X extraction of UO_2^{2+} – 71.6% relative to pre-X (Fig. 3c) – compared to the 1.25 equiv extraction (Fig. 3b). While no significant changes in Nd^{3+}, Sm^{3+}, and Cs^+ concentrations were observed here relative to the controls, we did observe a slight decrease in Th^{4+} concentration (9.2% vs. pre-X) which was greater than the control (1.6%) and beyond the detection error limit. While these data suggest that ^{PO}Cb²⁻ may drive the extraction of some Th^{4+} under these higher ratios, the selectivity for UO_2^{2+} under these conditions still dominates, as evidenced by the calculated separation factor (*SF*), derived from the distribution ratios of metals: $SF_{U/Th}$ = 25.[28]

In each experiment, the organic phases were analyzed by $^{31}P\{^1H\}$ NMR spectroscopy prior to GBE, following GBE, following extraction (post-X stage), following GBE discharge (*vide infra*), and following back-X (see Figs. S2-S4 for representative spectra). A representative post-X spectrum is shown in Fig. 3d and revealed the formation of (integrated

ratios relative to initially formed ^{PO}Cb²⁻ are in parentheses): a main product at 52.0 ppm (54%), residual ^{PO}Cb (18%), and minor new byproduct peaks (28%) (*vide infra*, Fig. 3d). The main new resonance at 52.0 ppm in DCE matches the chemical shift of the *bis*-carborane complex, **[CoCp*₂]₂[UO₂(^{PO}Cb)₂]**, in MeCN-d_3 and referenced to [PPN]⁺ (this salt is insoluble in DCE). Given that the calculated ICP-OES-determined quantity of captured UO_2^{2+} is 0.50 equiv and 0.49 equiv relative to the electrochemically generated ^{PO}Cb²⁻ (1.0 equiv) for the buffered 1.25 equiv (Fig. 3b) and 0.60 equiv (Fig. 3c) reactions, respectively, we propose that the resonance at 52.0 ppm most likely represents the *bis*-ligated anion, **[UO₂(^{PO}Cb)₂]²⁻**. Together, these results indicate that electrochemically generated ^{PO}Cb²⁻ *selectively* captures UO_2^{2+} from a mixed alkali, lanthanide, and actinide aqueous phase. While the nature of this selectivity remains under investigation, we suspect that optimal covalent bonding interactions between the P=O units and the U center – very recently investigated in the PUREX context[29, 30] – are likely at play.

In addition to this selective capture, these biphasic experiments revealed the formation of minor byproduct resonances in the $^{31}P\{^1H\}$ NMR spectrum of the DCE phase at 28.6 and 25.8 ppm (Fig. 3d). These resonances consistently had a 1:1 ratio suggesting that this may be a single product with inequivalent P centers. We also observed that these resonances became dominant when mixing a DCE solution of ^{PO}Cb²⁻ with an aqueous buffered phase in the absence of additional metal. Thus, treatment of a DCE solution containing **[Bu₄N]₂[^{PO}Cb]** to the NaOAc-buffered aqueous solution *without* additional metals cleanly generated the byproduct, along with residual ^{PO}Cb. The unknown byproduct was isolated by separation of the DCE phase, removal of the solvent, and selective crystallization by vapor diffusion of pentane into a saturated THF solution of the crude mixture. Analysis of the colorless single crystals by XRD studies revealed the formation of the protonated, monoanionic carborane species, **[Bu₄N][^{PO}CbH]** (Fig. 3g), featuring protonation at one of the *nido*-carborane C centers. The H1 atom at C1 was located in the difference map and was further observed by ^1H and ^1H-^{13}C HSQC NMR spectroscopy (Fig. 3f). The distinctly different geometries at C1 versus C2 leads to the observed asymmetry in the product and is responsible for the distinct ^{31}P NMR resonances observed. To the best of our knowledge, this is the first example of protonation of the *ortho*-substituted *nido*-carborane unit, [1,2-L₂-1,2-$C_2B_{10}H_{12}$]²⁻, at one of its C centers.

The release of extracted UO_2^{2+} was next probed electrochemically (Fig. 1b). The DCE phase containing the extracted UO_2^{2+} was separated from the aqueous phase and returned to the H-cell where it was galvanostatically discharged to achieve a theoretical final SOC of ca. 0% (Fig. S6). The DCE layer was next removed from the H-cell and a fresh, buffered (0.1 M NaOAc) or non-buffered aqueous solution was mixed with it rapidly for 15 h. Analysis of the aqueous layer by ICP-OES revealed the back-X of 22-38% of UO_2^{2+} relative to post-X values, with similar values observed regardless of the use of

buffered or non-buffered aqueous solutions (Fig. 3a-c). The highest UO_2^{2+} back-X observed were in the 0.6 equiv separations (ca. 38%), wherein concurrent back-X of Th^{4+} was also observed, albeit in smaller quantities (ca. 16%) relative to post-X (Fig. 3c). With the exception of this case, the back-X of all metals except UO_2^{2+} was negligible compared to the controls. Further analysis of the DCE layer by $^{31}P\{^1H\}$ NMR spectroscopy revealed the conversion back to the starting *closo*-carborane, **POCb** (Fig. 3e), as well as a minor unknown byproduct at 20.2 ppm (ca. 10% of total carborane peaks). These results demonstrate the electrochemical back-X of selectively captured UO_2^{2+} to an aqueous phase.

Conclusion

In summary, we have demonstrated the selective biphasic electrochemical capture and release of UO_2^{2+} from mixed-metal aqueous media using the redox-switchable **POCb/POCb²⁻** system. This system may offer a unique, electrochemical, non-stoichiometric extraction platform – distinguished from current PUREX technology – for UO_2^{2+} separation. Further studies are underway to further optimize this proof-of-principle system and to probe the origin of this selectivity, as well as to expand the mixed-metal system and better mimic SNF mixtures. New metal capture and release chemistry of energy importance is also being investigated.

Conflicts of interest

There are no conflicts to declare.

Acknowledgements

References

1.   IAEA, Nuclear Power and the Paris Agreement, https://www.iaea.org/sites/default/files/16/11/np-parisagreement.pdf, Accessed 2/5/2021, 2021.

2.   A. Adamantiades and I. Kessides, *Energ. Policy*, 2009, **37**, 5149-5166.

3.   D. J. Rose, *Science*, 1974, **184**, 351-359.

4.   I. Kumari, B. V. R. Kumar and A. Khanna, *Nucl. Eng. Des.*, 2020, **358**, 110410.

5.   W. B. Lanham and T. C. Runion (1949). *Purex Process for Plutonium and Uranium Recovery* (No. ORNL-479 (Del.)). Oak Ridge National Lab, USA

6.   J.-P. Glatz, in *Comprehensive Nuclear Materials (Second Edition)*, eds. R. J. M. Konings and R. E. Stoller, Elsevier, Oxford, 2020, pp. 305-326.

7.   P. Carbol, D. H. Wegen, T. Wiss, P. Fors, C. Jegou and K. Spahiu, in *Comprehensive Nuclear Materials (Second Edition)*, eds. R. J. M. Konings and R. E. Stoller, Elsevier, Oxford, 2020, pp. 347-386.

8.   M. Keener, C. Hunt, T. G. Carroll, V. Kampel, R. Dobrovetsky, T. W. Hayton and G. Ménard, *Nature*, 2020, **577**, 652-655.

9.   Y. Wu, X. Zhang, S.-Y. Kim and Y. Wei, *J. Nucl. Sci. Technol.*, 2016, **53**, 1968-1977.

10.   M. A. Denecke, N. Bryan, S. Kalmykov, K. Morris and F. Quinto, in *Experimental and Theoretical Approaches to Actinide Chemistry*, eds. J. K. Gibson and W. A. Jong, Wiley, 2018, pp. 378-444.

11.   F. Lahrouch, O. Sofronov, G. Creff, A. Rossberg, C. Hennig, C. Den Auwer and C. Di Giorgio, *Dalton Trans.*, 2017, **46**, 13869-13877.

12.   P. A. Bingham, R. J. Hand, M. C. Stennett, N. C. Hyatt and M. T. Harrison, *MRS Proceedings*, 2011, **1107**, 421.

13.   A. E. V. Gorden, J. Xu, K. N. Raymond and P. Durbin, *Chem. Rev.*, 2003, **103**, 4207-4282.

14.   N. S. Hosmane, T. Demissie, H. Zhang, J. A. Maguire, W. N. Lipscomb, F. Baumann and W. Kaim, *Organometallics*, 1998, **17**, 293-295.

15.   A. R. Oki, O. Sokolova, B. Gilbes, A. Aduroja, G. Abdelaziz and T. J. Emge, *Inorg. Chem. Commun.*, 2002, **5**, 694-697.

16.   R. Neufeld, R. Michel, R. Herbst-Irmer, R. Schöne and D. Stalke, *Chem. Eur. J.*, 2016, **22**, 12340-12346.

17.   A. I. Ojeda-Amador, A. J. Martínez-Martínez, A. R. Kennedy and C. T. O'Hara, *Inorg. Chem.*, 2016, **55**, 5719-5728.

18.   J.-C. Berthet, M. Nierlich and M. Ephritikhine, *Polyhedron*, 2003, **22**, 3475-3482.

19.   Z. Spichal, M. Necas, J. Pinkas and Z. Zdrahal, *Polyhedron*, 2006, **25**, 809-814.

20.   K. Miyata, T. Nakagawa, R. Kawakami, Y. Kita, K. Sugimoto, T. Nakashima, T. Harada, T. Kawai and Y. Hasegawa, *Chem. Eur. J.*, 2011, **17**, 521-528.

21.   Y.-Z. Pan, Q.-Y. Hua, L.-S. Lin, Y.-B. Qiu, J.-L. Liu, A.-J. Zhou, W.-Q. Lin and J.-D. Leng, *Inorg. Chem. Front.*, 2020, **7**, 2335-2342.

22.   I. Korobkov, A. Arunachalampillai and S. Gambarotta, *Organometallics*, 2004, **23**, 6248-6252.

23.   A.-G. D. Nelson, T. H. Bray, F. A. Stanley and T. E. Albrecht-Schmitt, *Inorg. Chem.*, 2009, **48**, 4530-4535.

24.   J. Diwu, J. J. Good, V. H. DiStefano and T. E. Albrecht-Schmitt, *Eur. J. Inorg. Chem.*, 2011, **2011**, 1374-1377.

25.   F. Quilès, C. Nguyen-Trung, C. Carteret and B. Humbert, *Inorg. Chem.*, 2011, **50**, 2811-2823.

26.   D. D. Pant and D. P. Khandelwal, *P. Indian Acad. Sci. A*, 1959, **50**, 323-335.

27.   C. Hunt, M. Mattejat, C. Anderson, L. Sepunaru and G. Ménard, *ACS Appl. Energy Mater.*, 2019, **2**, 5391-5396.

28.   N. A. Thiele, D. J. Fiszbein, J. J. Woods and J. J. Wilson, *Inorg. Chem.*, 2020, **59**, 16522-16530.

29.   D. Raychaudhuri, G. Gopakumar, S. Nagarajan and C. V. S. Brahmmananda Rao, *J. Phys. Chem. A*, 2020, **124**, 7805-7815.

30.   Y. Zhang, W. Duan, Y. Yang, T. Jian, Y. Qiao, G. Ren, N. Zhang, L. Zheng, W. Yan, J. Wang, J. Chen, S. G. Minasian and T. Sun, *Inorg. Chem.*, 2022, **61**, 92-104.